J Electr Eng Technol.2017; 12(6): 2237-2246
http://doi.org/10.5370/JEET.2017.12.6.2237

ISSN(Print) 1975-0102
ISSN(Online) 2093-7423

Nonisolated Two-Phase Bidirectional DC-DC Converter with Zero-Voltage-Transition for Battery Energy Storage System

Chang-Soon Lim* and Kui-Jun Lee†

Abstract – A nonisolated two-phase bidirectional dc-dc converter (NTPBDC) is a very attractive solution for the battery energy storage system (BESS) applications due to the high voltage conversion ratio and the reduced conduction loss of the switching devices. However, a hard-switching based NTPBDC decreases the overall voltage conversion efficiency. To overcome this problem, this paper proposes a novel NTPBDC with zero-voltage-transition (NTPBDC -ZVT). The soft-switching for the boost and buck main switches is achieved by using a resonant cell, which consists of a single resonant inductor and four auxiliary switches. Furthermore, due to the single resonant inductor, the proposed NTPBDC-ZVT has the advantages of simple implementation, reduced size, and low cost. The validity of the proposed NTPBDC-ZVT is verified through experimental results.

Keywords: Bidirectional dc-dc converter, Zero-Voltage-Transition (ZVT), Battery Energy Storage System (BESS)

1. Introduction

In recent years, the global energy crisis has been intensified by the rapidly growing economy and the resulting great demand for energy. Renewable energy systems, such as photovoltaic (PV) and wind energy, are currently considered to be promising solutions to this problem, so they are widely used and studied all over the world. However, since PV and wind power intrinsically vary with time, weather, and environment, it is difficult to achieve sufficient and predictable power from renewable power sources [1-3]. Energy storage systems (ESSs) are typically used to solve these problems of PV and wind power. ESSs provide significant enhancements of power quality, stability, and reliability to the grid [4]. Among ESSs, the battery energy storage system (BESS), with the advantages of high energy density, long lifespan, and low initial cost, is one of the most widely used [5, 6].

In a BESS, series-connected battery strings (SCBSs) are generally used to achieve the high power requirements. However, since each battery cell connected in series has different chemical and electrical characteristics, imbalances among battery cells are generated by repeated charge and discharge processes. Such imbalanced battery states severely decrease the energy storage capacity and battery lifetime [7-9]. To minimize these problems, the SCBSs should not be too long. For this reason, voltage levels of the SCBSs are typically much lower than the dc-bus voltage. Although parallel-connected battery strings (PCBSs) alleviate these problems of the SCBSs, the voltage levels of the PCBSs are also much lower than the dc-bus voltage [10, 11]. Therefore, bidirectional dc-dc converters (BDCs) with high conversion ratio are required for charging and discharging the battery strings.

Numerous BDCs have been developed, which can be categorized as isolated and nonisolated types. Isolated bidirectional dc-dc converters (IBDCs), which include half-bridge [12-14] and full-bridge types [15-18], can provide high step-up and step-down voltage gains by adjusting the turns ratio of the transformer. The isolated types are also used when the low and high voltage sides cannot be grounded simultaneously. However, IBDCs suffer from high voltage spikes on the switching devices due to the unavoidable leakage inductance of the power transformer. To overcome this drawback, some literatures have presented various methods to clamp the voltage spikes on the switching devices and to recycle the energy of leakage inductance [19-22].

Nonisolated bidirectional dc-dc converters (NBDCs), which include conventional buck/boost [23-26], three-level [27], multilevel [28], sepic/zeta [29], switched capacitor [30], and coupled inductor types [31], generally provide simple structures and control schemes. Therefore, applications using the NBDCs can achieve relatively high efficiency, high power density, and low cost [32]. However, the NBDCs have several limitations and problems. The conventional buck/boost and three-level types cannot achieve high conversion ratios. The multilevel type does not include an inductor, but uses 12 switches. If a higher conversion ratio is required, more switches are needed. In the sepic/zeta type, the system efficiency is low because two power stages are combined. Although the switched capacitor and coupled inductor types achieve high conversion ratios, their circuit configurations are complicated.

† Corresponding Author: Dept. of Electrical Engineering, Korea National University of Transportation, Korea. (kuijun.lee@ut.ac.kr)
* Mechatronics R&D Center, Samsung Electronics Company, Ltd., Hwaseong, Korea. (cslim911@naver.com)
Received: March 20, 2017; Accepted: July 17, 2017

Also, for the NBDCs in [27-31], it is difficult to apply the multi-phase concept compared with the conventional buck/boost type due to a circuit complexity. Therefore, they are not suitable for high current applications.

In contrast to the NBDCs in [23-31], a nonisolated two-phase bidirectional dc-dc converter (NTPBDC), which consists of a current doubler and a voltage doubler, is a very attractive solution for the BESS. The configuration and operation of the NTPBDC are simple and the NTPBDC provides a much higher conversion ratio without using a switched capacitor or coupled inductor. Since the current doubler divides the current into two inductor currents, the NTPBDC can reduce the copper loss of the inductors and the conduction loss of the switching devices. Furthermore, the inductor current ripple can be reduced by applying an interleaved control scheme. To minimize the filter size and weight, high-frequency switching operation of the NTPBDC is desirable. However, in the hard-switching NTPBDC, when the switching frequency increases, switching loss and electromagnetic interference (EMI) noise increase. To overcome these drawbacks, a soft-switching technique is required.

This paper proposes a novel NTPBDC with zero-voltage-transition (NTPBDC-ZVT) for the BESS. To achieve zero-voltage-switching (ZVS) for the boost and buck main switches without increasing their voltage and current stresses, the proposed NTPBDC-ZVT utilizes a resonant cell, which consists of a single resonant inductor and four auxiliary switches. Due to the single resonant inductor, the proposed NTPBDC-ZVT has the advantages of simple implementation and reduced size. A 1kW prototype of the proposed NTPBDC-ZVT has been built and successfully tested under a full load, and the experimental results are provided to verify the effectiveness of the proposed NTPBDC-ZVT.

2. Proposed Converter

2.1 System configuration

Fig. 1 shows the conventional NTPBDC. The low voltage side consists of two boost main switches S_1 and S_2, two inductors L_1 and L_2, and a capacitor C_{L1}. The high voltage side includes two buck main switches S_3 and S_4 and two capacitors C_{H1} and C_{H2}. Due to the series-connected capacitors C_{H1} and C_{H2}, the high voltage side of the circuit is configured as a voltage doubler rectifier that obtains a high step-up voltage gain.

Fig. 2 shows the proposed NTPBDC-ZVT, which consists of the conventional NTPBDC and a resonant cell. The resonant cell is comprised of a single resonant inductor L_r and four auxiliary switches S_5, S_6, S_7, and S_8. Since the resonant cell operates only during small interval across entire one switching period T_S, low current rating devices can be used for the four auxiliary switches so the additional

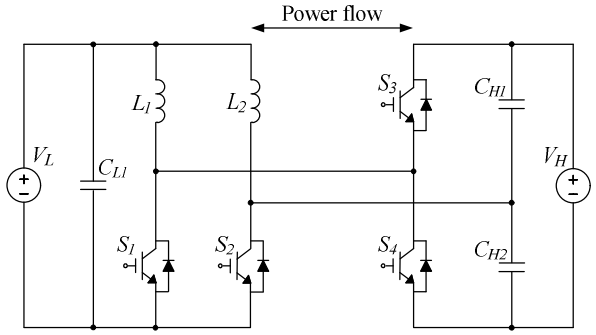

Fig. 1. Conventional NTPBDC

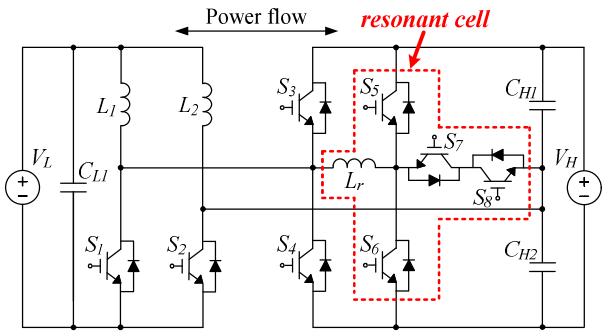

Fig. 2. Proposed NTPBDC-ZVT.

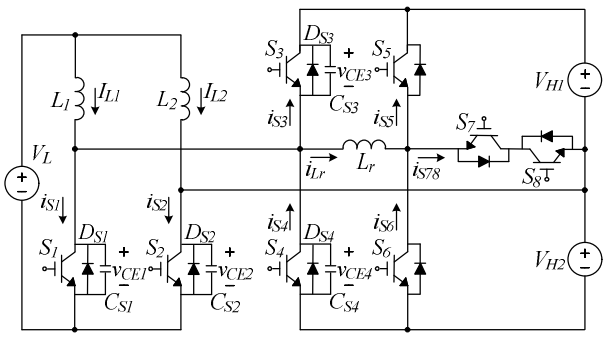

Fig. 3. Simplified circuit diagram of the proposed NTPBDC-ZVT

switching loss from that cannot be comparable with the reduced main switching loss obtained from ZVS.

To simplify the analysis for boost and buck operation modes, C_{L1}, C_{H1}, and C_{H2} have been replaced by voltage sources V_L, V_{H1}, and V_{H2}, respectively, as shown in Fig. 3, under the following assumptions.

1) All main and auxiliary switches are ideal, i.e., they represent zero impedance while in the turn-on state and infinite impedance while in the turn-off state.

2) The capacitors C_{S1}, C_{S2}, C_{S3}, and C_{S4} are the sum of the parasitic capacitors of the main switches S_1, S_2, S_3, and S_4 and external added capacitors.

3) The parasitic capacitors of the auxiliary switches are neglected.

4) Inductors L_1 and L_2 have large inductance values and their currents are identical constants, i.e., $I_{L1} = I_{L2}$.

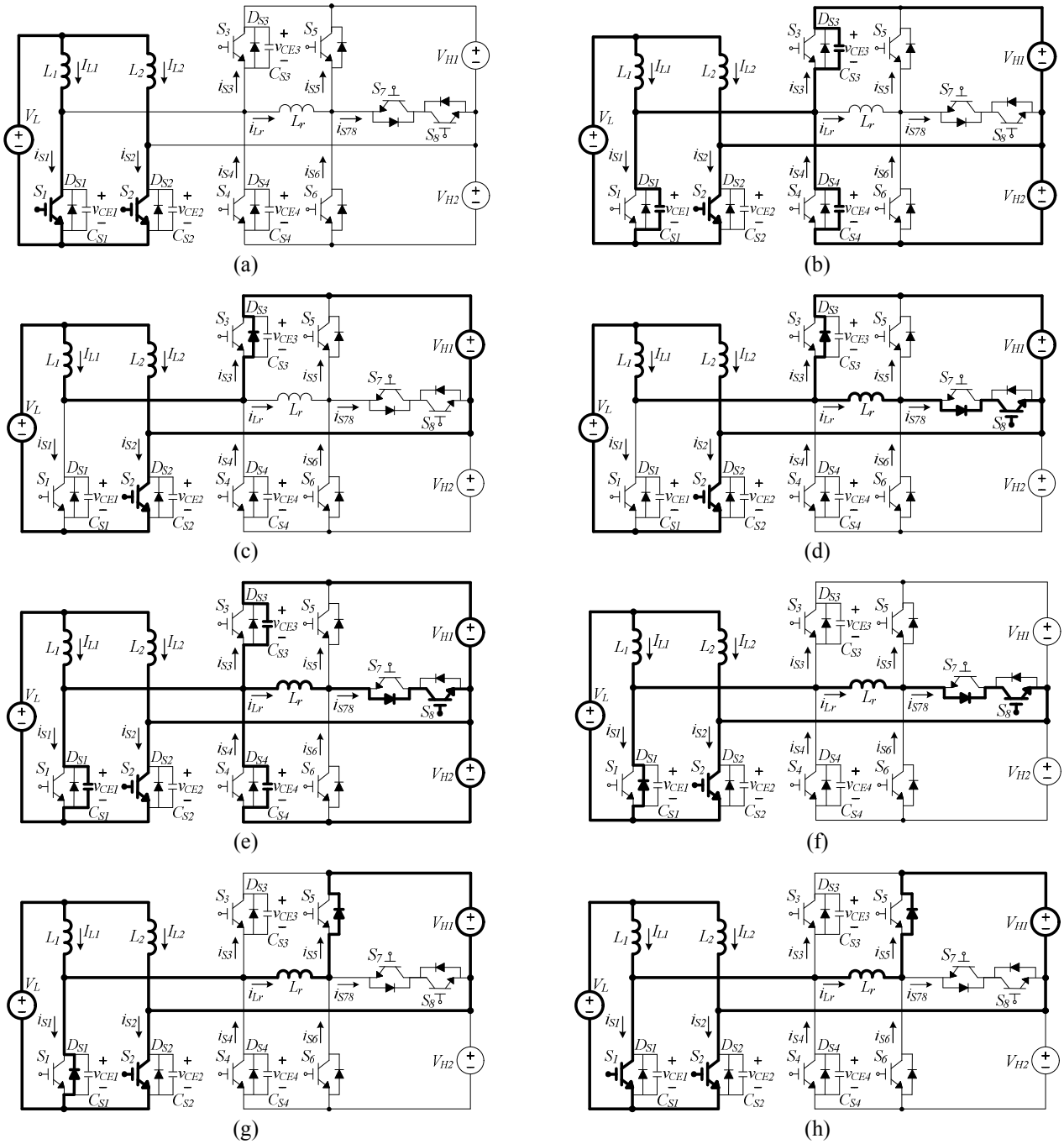

Fig. 4. Operating modes of the proposed NTPBDC-ZVT in the boost state. (a) Mode 1(t_0 - t_1). (b) Mode 2(t_1 - t_2). (c) Mode 3(t_2 - t_3). (d) Mode 4(t_3 - t_4). (e) Mode 5(t_4 - t_5). (f) Mode 6(t_5 - t_6). (g) Mode 7(t_6 - t_7). (h) Mode 8(t_7 - t_8)

5) Capacitors C_{L1}, C_{H1}, and C_{H2} are large enough to neglect the voltage ripple and V_{H1} and V_{H2} are identical constants, i.e., $V_{H1} = V_{H2}$.

2.2 Operation mode analysis for boost state

Fig. 4 shows the operating modes of the proposed NTPBDC-ZVT in the boost state during the half switching period T_S /2, and Fig. 5 shows the theoretical waveforms of the proposed NTPBDC-ZVT in the boost state during one switching period T_S. The steady-state operation of the proposed NTPBDC-ZVT in the boost state includes a total of 16 modes for one switching period. However, due to the symmetrical operation of the proposed NTPBDC-ZVT, only 8 leading modes in the boost state are analyzed.

1) ***Mode 1*** ($t_0 - t_1$): During this interval, two boost main switches S_1 and S_2 are turned on. They are identical to the charging mode of the basic boost converter.

2) ***Mode 2*** ($t_1 - t_2$): At t_1, S_1 is turned off and the

capacitor C_{S1} is linearly charged. At the same time, capacitors C_{S3} and C_{S4} are linearly discharged and charged, respectively.

3) ***Mode 3*** ($t_2 - t_3$): At t_2, the voltages V_{CE1} and V_{CE4} become V_{H1} and V_H, respectively. During this interval, the energy stored in inductor L_1 is transferred to the load through the anti-parallel diode of S_3 and it is identical to the discharging mode of the basic boost converter. The current of switch S_2 (i.e., i_{S2}) is then the sum of I_{L1} and I_{L2}.

4) ***Mode 4*** ($t_3 - t_4$): At t_3, the auxiliary switch S_8 is turned on, and then resonant inductor current i_{Lr} ramps up linearly until it reaches I_{L1} at t_4. At the same time, the current of the anti-parallel diode of S_3 (i.e., i_{S3}) decreases linearly to zero and it turns off softly with a zero-current-switching (ZCS) condition. The time interval t_{34} of mode 4 is given by

$$t_{34} = \frac{I_{L1}}{V_{H1} / L_r} \tag{1}$$

5) ***Mode 5*** ($t_4 - t_5$): The resonant inductor current i_{Lr} continues to increase due to the resonance of L_r, C_{S1}, C_{S3}, and C_{S4}. During this interval, C_{S1} is discharged until the voltage v_{CE1} decreases to zero. At the same time, C_{S3} and C_{S4} are charged and discharged, respectively. The resonant time period t_{45} is

$$t_{45} = \frac{\pi}{2}\sqrt{L_r C_r} \tag{2}$$

where $C_r = C_{S1} + C_{S3} + C_{S4}$.

6) ***Mode 6*** ($t_5 - t_6$): At t_5, the current i_{S1} flows negatively through anti-parallel diode D_{S1}, and the currents i_{S2} is more than the sum of I_{L1} and I_{L2} because of the added resonant inductor current i_{Lr}. To achieve the ZVS, the turn-on gating signal of S_1 should be applied while the anti-parallel diode D_{S1} of S_1 is conducting. The time delay T_D between S_8 and S_1 gate signals must satisfy the following

$$T_D \geq t_{34} + t_{45} = \frac{I_{L1}}{V_{H1} / L_r} + \frac{\pi}{2}\sqrt{L_r C_r} \tag{3}$$

7) ***Mode 7*** ($t_6 - t_7$): At t_6, the auxiliary switch S_8 is turned off, and then the energy stored in resonant inductor L_r is transferred to the load through the anti-parallel diode of S_5. The resonant inductor current i_{Lr} decreases linearly to I_{L1}, the current i_{S1} increases linearly to zero, and the current i_{S2} decreases linearly to the sum of I_{L1} and I_{L2}.

8) ***Mode 8*** ($t_7 - t_8$): From t_7, the current i_{S1} flows positively through S_1. During this interval, the resonant inductor current i_{Lr} decreases linearly to zero, the current i_{S1} increases linearly to I_{L1}, and the current i_{S2} decreases linearly to I_{L2}.

The lagging 8 operation modes (i.e., from mode 9 to mode 16) are symmetric with the aforementioned modes (i.e., from mode 1 to mode 8). At t_{16}, the operating mode changes to mode 1 in the next switching period.

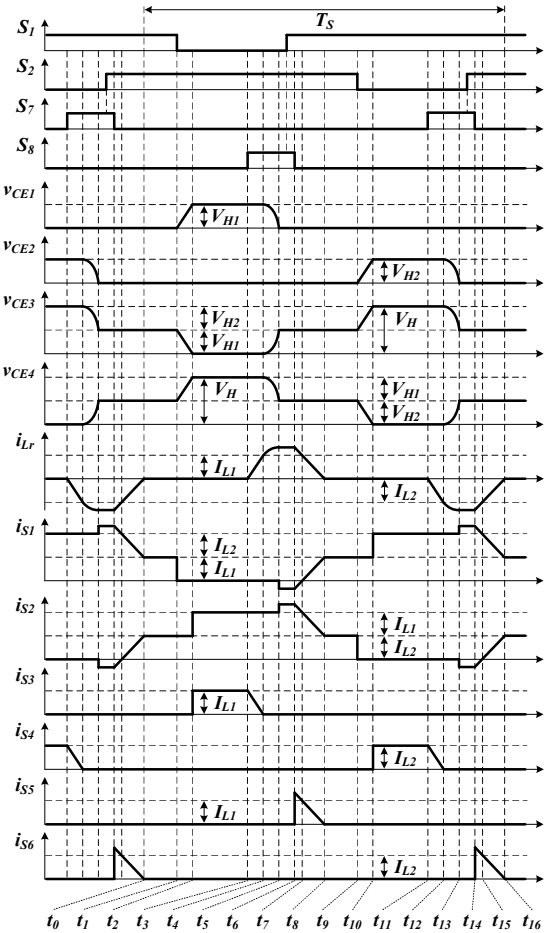

Fig. 5. Theoretical waveforms of the proposed NTPBDC-ZVT in the boost state

2.3 Operation mode analysis for buck state

Fig. 6 shows the operating modes of the proposed NTPBDC- ZVT in the buck state during the half switching period T_S /2, and Fig. 7 shows the theoretical waveforms of the proposed NTPBDC-ZVT in the buck state during one switching period T_S. The steady-state operation of the proposed NTPBDC-ZVT in the buck state includes a total of 16 modes for one switching period. However, due to the symmetrical operation of the proposed NTPBDC-ZVT, only 8 leading modes in the buck state are analyzed.

1) ***Mode 1*** ($t_0 - t_1$): During this interval, two buck main switches S_3 and S_4 are turned off. They are identical to the discharging mode of the basic buck converter.

2) ***Mode 2*** ($t_1 - t_2$): At t_1, the auxiliary switch S_5 is turned on, and then resonant inductor current i_{Lr} decreases linearly to - I_{L1}. At the same time, the current of the anti-parallel diode of S_1 decreases linearly to zero (i.e., i_{S1} increases linearly to zero) and it turns off softly with the ZCS condition. The time interval t_{12} of mode 2 is identical to (1).

3) ***Mode 3*** ($t_2 - t_3$): At t_2, the current i_{S2} is the sum of - I_{L1} and - I_{L2}, and then the resonant inductor current i_{Lr}

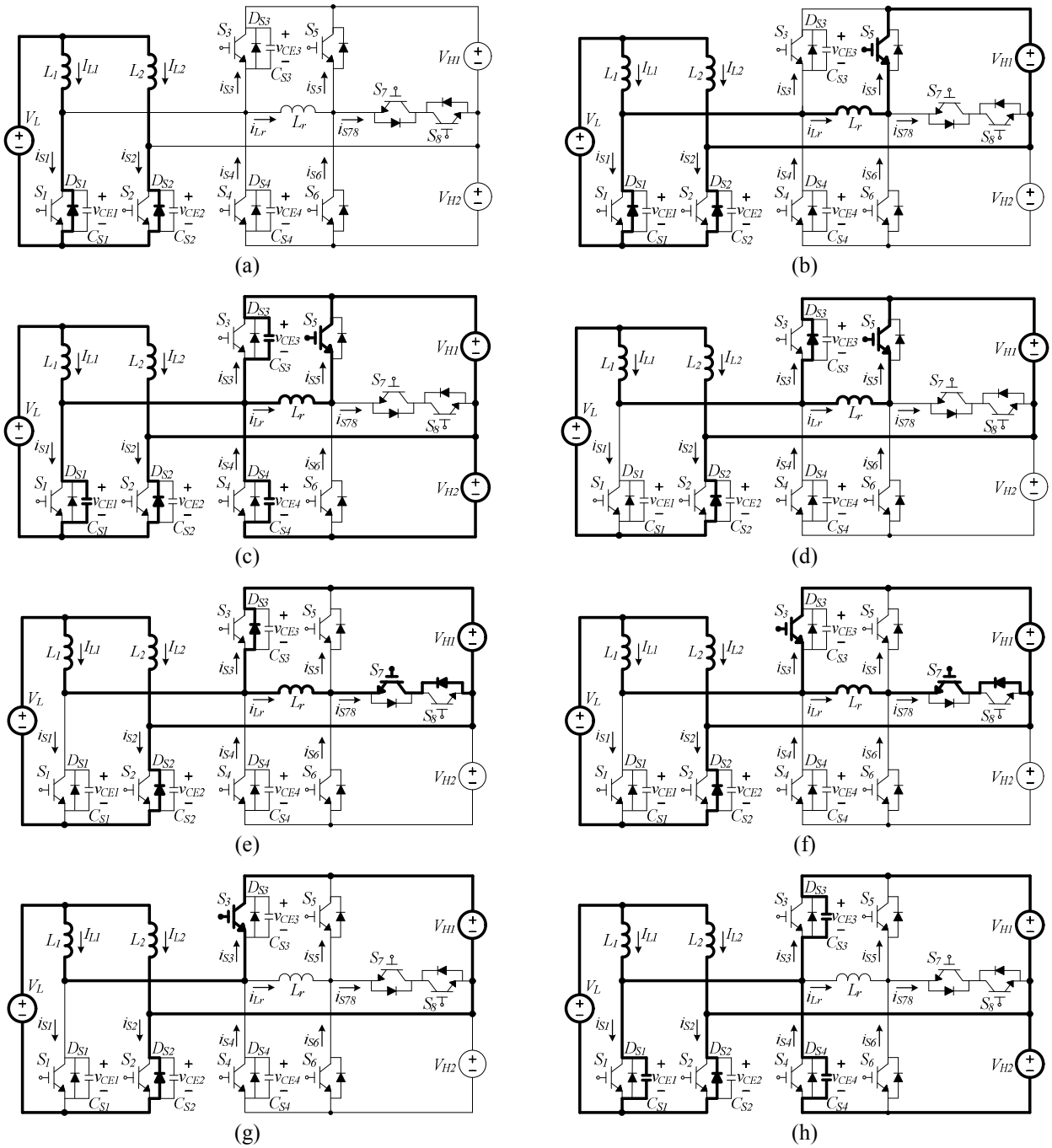

Fig. 6. Operating modes of the proposed NTPBDC-ZVT in the buck state. (a) Mode 1(t_0 - t_1). (b) Mode 2(t_1 - t_2). (c) Mode 3(t_2 - t_3). (d) Mode 4(t_3 - t_4). (e) Mode 5(t_4 - t_5). (f) Mode 6(t_5 - t_6). (g) Mode 7(t_6 - t_7). (h) Mode 8(t_7 - t_8)

continues to decrease due to the resonance of L_r, C_{S1}, C_{S3}, and C_{S4}. During this interval, C_{S1} is charged until the voltage v_{CE1} increases to V_{H1}. At the same time, C_{S3} and C_{S4} are discharged and charged, respectively. The resonant time period t_{23} is identical to (2).

4) ***Mode 4*** ($t_3 - t_4$): At t_3, the current i_{S3} flows positively through anti-parallel diode D_{S3} of S_3. To achieve the ZVS, the turn-on gating signal of S_3 should be applied while the anti-parallel diode D_{S3} of S_3 is conducting. The time delay T_D between the S_5 and S_3 gate signals is identical to (3). Before S_5 is turned off (i.e., before starting mode 5), the turn-on gating signal of S_7 should be applied. Therefore, although S_5 is turned off, the resonant inductor current i_{Lr} can flow continuously.

5) ***Mode 5*** ($t_4 - t_5$): At t_4, S_5 is turned off, and then the energy stored in resonant inductor L_r is transferred to the V_{H1} through S_7 and the anti-parallel diode of S_8. The resonant inductor current i_{Lr} increases linearly to - I_{L1}, and the current i_{S3} decreases linearly to zero.

6) ***Mode 6*** ($t_5 - t_6$): From t_5, the current i_{S3} flows

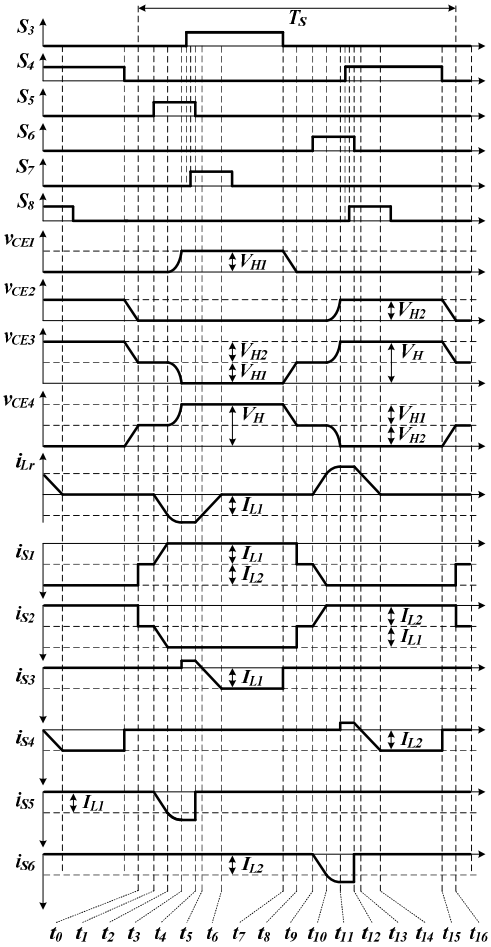

Fig. 7. Theoretical waveforms of the proposed NTPBDC-ZVT in the buck state

negatively through S_3, and then the energy stored in resonant inductor L_r is transferred to the load through S_7 and the anti-parallel diode of S_8. During this interval, the resonant inductor current i_{Lr} increases linearly to zero, and the current i_{S3} decreases linearly to - I_{L1}.

7) ***Mode 7*** ($t_6 - t_7$): At t_6, the current i_{S3} becomes - I_{L1}, and it is identical to the charging mode of the basic buck converter. Since the resonant inductor current i_{Lr} becomes zero, the turn-off gating signal of S_7 should be applied.

8) ***Mode 8*** ($t_7 - t_8$): At t_7, S_3 is turned off and the capacitor C_{S3} is linearly charged. At the same time, both capacitors C_{S1} and C_{S4} are linearly discharged.

As the boost operation, the lagging 8 operation modes (i.e., from mode 9 to mode 16) are symmetric with the aforementioned modes (i.e., from mode 1 to mode 8). At t_{16}, the operating mode changes to mode 1 in the next switching period.

2.4 Duty ratio and voltage conversion ratio

The NTPBDC-ZVT has different operating ranges of the duty ratio, depending on the state. In the boost state, the two boost main switches S_1 and S_2 should not be turned off simultaneously. When both S_1 and S_2 are turned off, the current paths of the two inductors L_1 and L_2 are not provided, and then high voltage spikes appear at the terminals of the inductors. Such high voltage spikes would cause the two boost main switches to be permanently damaged. To avoid these problems, the duty ratio D_{12} for the two boost main switches should be above a 0.5 duty ratio. The NTPBDC-ZVT can obtain double the high-side voltage of the basic boost converter. Therefore, the voltage conversion ratio in the boost state should be

$$\frac{V_H}{V_L} = \frac{2}{1 - D_{12}} > 4 \tag{4}$$

In the buck state, the two buck main switches S_3 and S_4 should not be turned on simultaneously. If both S_3 and S_4 were turned on, a short circuit would occur and destroy the switching devices. To avoid a short circuit, the duty ratio D_{34} for the two buck main switches should be under a 0.5 duty ratio. The NTPBDC-ZVT can obtain half the low-side voltage of the basic buck converter. Therefore, the voltage conversion ratio in the buck state should be

$$\frac{V_L}{V_H} = \frac{D_{34}}{2} < 0.25 \tag{5}$$

2.5 Design guide of resonant components L_r and C_r

1) ***Resonant Inductor L_r*** : The resonant inductor L_r affects the reverse-recovery phenomenon of the anti-parallel diodes of the four main switches (S_1, S_2, S_3, and S_4). So, to minimize the reverse- recovery effects and to achieve the ZCS turn-off of those anti-parallel diodes, the resonant inductor value should be selected relevantly. In this paper, the rising time of i_{Lr} from 0 to I_{L1} or I_{L2} is chosen to be twice the reverse-recovery time t_{rr} of those anti-parallel diodes, and the resonant inductance is obtained as follows from (1)

$$L_r = \frac{2 t_{rr} V_{H1}}{I_{L\_\min}} \tag{6}$$

where I_{L_min} is the minimum value of the inductor current.

2) ***Resonant Capacitor C_r*** : The resonant capacitor C_r is selected based on the maximum resonant current I_{Lr_peak} by

$$I_{Lr\_peak} = I_{L1} + \frac{V_{C1}}{Z_r}, \quad Z_r = \sqrt{\frac{L_r}{C_r}}. \tag{7}$$

If the resonant capacitor becomes large, it has advantage of limiting the *dv/dt* of the four main switches (S_1, S_2, S_3, and S_4) at turn-off. However, a large capacitor can increase the current I_{Lr_peak} and the related conduction losses so it

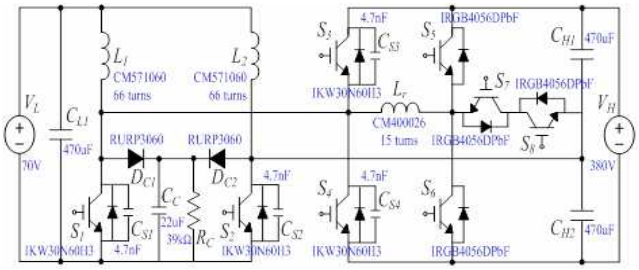

Fig. 8. Schematic diagram of the 1kW NTPBDC-ZVT

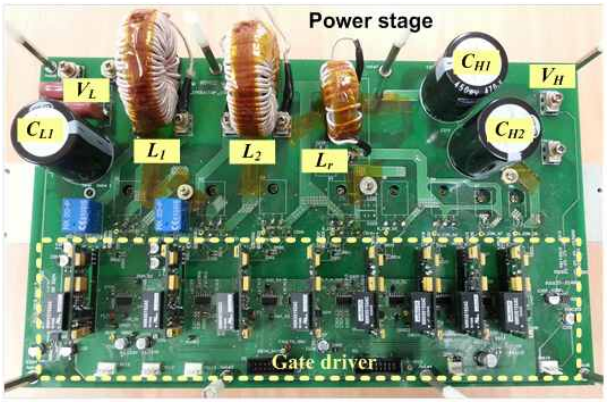

Fig. 9. Photograph of the experimental prototype

should be appropriately restricted. In this paper, the current I_{Lr_peak} is limited to 1.2 times the I_{L1}, and the resonant capacitance is given by

$$C_r = \frac{L_r\left(I_{Lr\_peak} - I_{L1}\right)^2}{V_{C1}^2}. \quad (8)$$

3. Experimental Results

To verify the theoretical operation and evaluate the performance, a 1kW prototype of the proposed NTPBDC-ZVT was built and tested. Fig. 8 shows a schematic diagram of the 1kW NTPBDC-ZVT, and Fig. 9 shows a photograph of the experimental prototype. IKW30N60H3 (V_{CE} = 600V, I_C = 30A, V_{CEsat}@25°C = 1.95V) IGBTs from Infineon were used for the boost main switches (S_1 and S_2) and buck main switches (S_3 and S_4). To obtain the desired inductance of inductors L_1 and L_2, each inductor consisted of the magnetic powder core (Chang Sung, CM571060) and 66 turns of magnet wire. To construct the resonant cell, IRGB4056DPbF (V_{CE} = 600V, I_C = 12A, V_{CEsat} @25°C = 1.55V) IGBTs from International Rectifier were used for the auxiliary switches S_5, S_6, S_7, and S_8, and the single resonant inductor L_r consisted of a magnetic powder core (Chang Sung, CM400026) and 15 turns of magnet wire. An additional RCD snubber circuit connected across the boost main switches was used to prevent voltage stress at turn-off.

Table 1. Experimental conditions

Parameters	Value
Output Power (P_O)	1 *kW*
Low-side Voltage (V_L)	70 *V*
High-side Voltage (V_H)	380 *V*
Switching Frequency (f_S)	40 *kHz*
Inductors (L_1, L_2)	500 *uH*
Resonant Inductor (L_r)	20 *uH*
Capacitors (C_{L1}, C_{H1}, C_{H2})	470 *uF*
Resonant Capacitors (C_{S1}, C_{S2}, C_{S3}, C_{S4})	4.7 *nF*

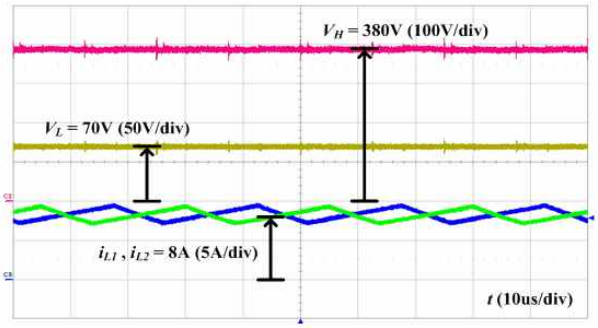

(a)

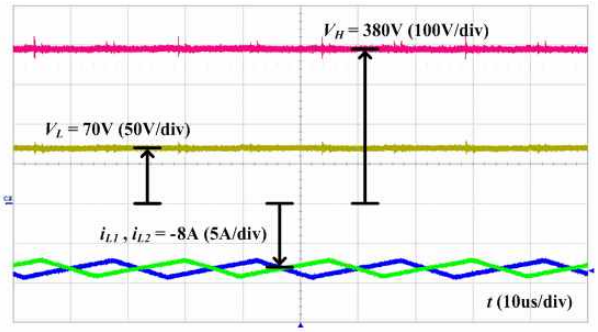

(b)

Fig. 10. Experimental results of the proposed NTPBDC-ZVT: (a) Waveforms in the boost state; (b) Waveforms in the buck state

The other experimental conditions are summarized in Table 1. Fig. 10 shows the steady-state waveforms of the low-side voltage V_L, high-side voltage V_H, and inductor currents i_{L1} and i_{L2} at 100% load; Fig. 10(a) shows the boost state, and Fig. 10(b) shows the buck state. The two-phase interleaved inductor currents in the boost and buck states have positive values (average current: 8A) and negative values (average current: -8A), respectively. Fig. 11 shows the ZVS waveforms of the gate-to-emitter voltage v_{GE1} of the boost main switch S_1, the resonant inductor current i_{Lr}, and the collector-to-emitter voltage v_{CE1} of S_1 at 100% load in the boost state. The waveforms of Fig. 11(b) are magnifications of the original waveforms of Fig. 11(a). The gate-to-emitter voltage v_{GE1} apparently turns on at a clear zero-voltage condition. Fig. 12 shows the ZVS waveforms of the gate-to-emitter voltage v_{GE3} of

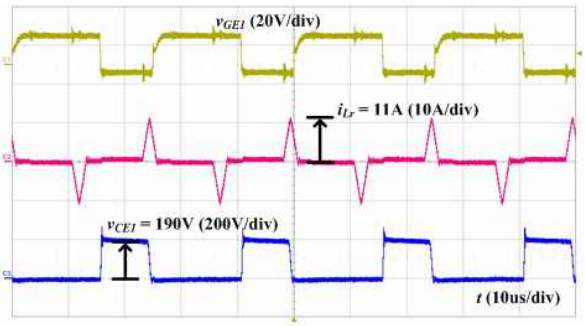

(a)

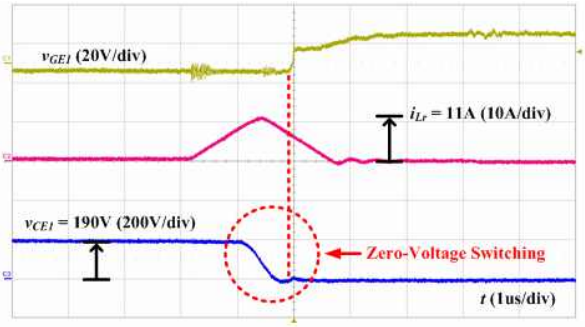

(b)

Fig. 11. Experimental results of the proposed NTPBDC-ZVT in the boost state: (a) Original ZVS waveforms; (b) Magnified ZVS waveforms of (a)

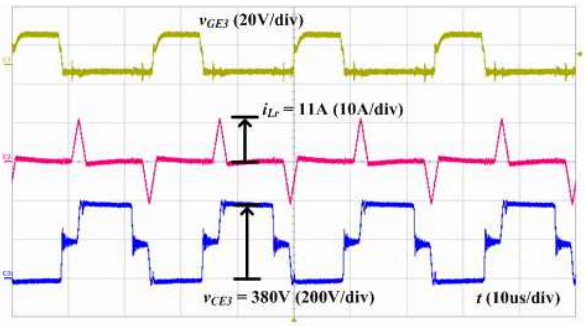

(a)

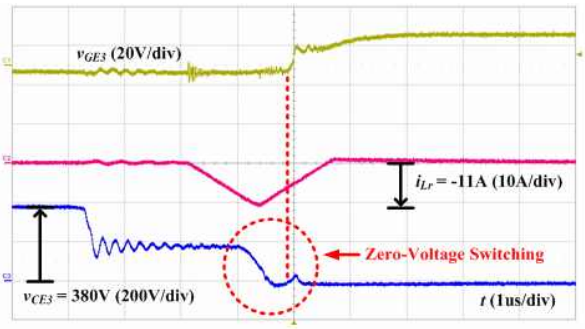

(b)

Fig. 12. Experimental results of the proposed NTPBDC-ZVT in the buck state. (a) Original ZVS waveforms. (b) Magnified ZVS waveforms of (a)

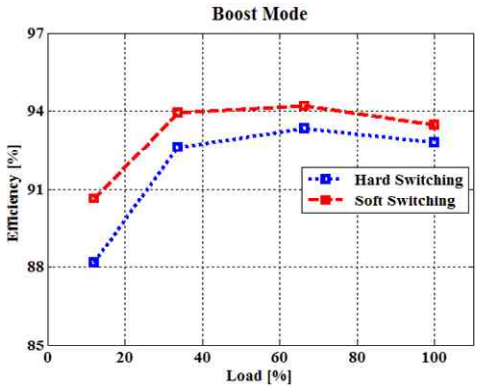

(a)

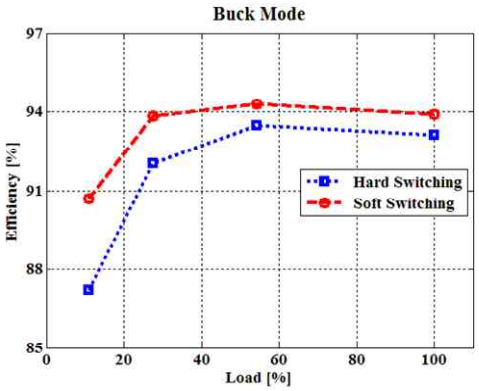

(b)

Fig. 13. Measured efficiency of the two switching techniques under load variation: (a) Boost state; (b) Buck state

the buck main switch S_3, the resonant inductor current i_{Lr}, and the collector-to-emitter voltage v_{CE3} of S_3 at 100% load in the buck state. The waveforms of Fig. 12(b) are magnifications of the original waveforms of Fig. 12(a). The gate-to-emitter voltage v_{GE3} apparently turns on at a clear zero-voltage condition. Fig. 13 shows the experimental efficiency measurement of the two switching techniques, hard-switching and soft-switching, under load variation in the boost and buck states. It can be seen that the soft-switching technique significantly improves the overall system efficiency in both the boost state and the buck state. Specifically, the efficiency improvement at light load condition is remarkable because the switching loss is dominant compared to the conduction loss.

4. Conclusions

In this paper, a novel NTPBDC-ZVT was proposed to satisfy high efficiency voltage conversion for BESS applications. Since soft-switching for both the boost and buck main switches is achieved by using a resonant cell, switching losses are reduced. Furthermore, the proposed NTPBDC-ZVT has the advantages of simple implementation

and reduced size due to the single resonant inductor. The steady-state analysis of the proposed NTPBDC-ZVT was discussed in detail and a 1kW prototype was built and tested in the laboratory. Experimental results demonstrate that the proposed NTPBDC-ZVT is an excellent candidate for use in BESS applications.

Acknowledgements

This was supported by Korea National University of Transportation in 2017.

References

[1] E. S. Sreeraj, K. Chatterjee, and S. Bandyopadhyay, "One-cycle-controlled single-stage single-phase voltage-sensorless grid- connected PV system," *IEEE Trans. Ind. Electron.*, vol. 60, no. 3, pp. 1216-1224, Mar. 2013.

[2] H. Beltran, E. Bilbao, E. Belenguer, I. Etxeberria-Otadui, and P. Rodriguez, "Evaluation of storage energy requirements for constant production in PV power plants," *IEEE Trans. Ind. Electron.*, vol. 60, no. 3, pp. 1225-1234, Mar. 2013.

[3] Y. Xia, K. H. Ahmed, and B. W. Williams, "Wind turbine power coefficient analysis of a new maximum power point tracking technique," *IEEE Trans. Ind. Electron.*, vol. 60, no. 3, pp. 1122-1132, Mar. 2013.

[4] X. Lu, K. Sun, J. M. Guerrero, J. C. Vasquez, and L. Huang, "State-of-Charge Balance Using Adaptive Droop Control for Distributed Energy Storage Systems in DC Microgrid Applications," *IEEE Trans. Ind. Electron.*, vol. 61, no. 6, pp. 2804-2815, Jun. 2014.

[5] B. Zhao, Q. Song, W. Liu, and Y. Sun, "A Synthetic Discrete Design Methodology of High-Frequency Isolated Bidirectional DC/DC Converter for Grid-Connected Battery Energy Storage System Using Advanced Components," *IEEE Trans. Ind. Electron.*, vol. 61, no. 10, pp. 5402-5410, Oct. 2014.

[6] Z. Ding, C. Yang, Z. Zhang, C. Wang, and S. Xie, "A Novel Soft-Switching Multiport Bidirectional DC-DC Converter for Hybrid Energy Storage System, " *IEEE Trans. Power Electron.*, vol. 29, no. 4, pp. 1595-1609, Apr. 2014.

[7] C. S. Lim, K. J. Lee, N. J. Ku, D. S. Hyun, and R. Y. Kim, "A Modularized Equalization Method Based on Magnetizing Energy for a Series-Connected Lithium-Ion Battery String," *IEEE Trans. Power Electron.*, vol. 29, no. 4, pp. 1791-1799, Apr. 2014.

[8] C.-H. Kim, M.-Y. Kim, H.-S. Park, and G.-W. Moon, "A modularized two-stage charge equalizer with cell selection switches for series-connected lithium-ion battery string in an HEV," *IEEE Trans. Power Electron.*, vol. 27, no. 8, pp. 3764-3774, Aug. 2012.

[9] C.-H. Kim, M.-Y. Kim, H.-S. Park, and G.-W. Moon, "A modularized charge equalizer using a battery monitoring IC for series-connected li-ion battery strings in electric vehicles," *IEEE Trans. Power Electron.*, vol. 28, no. 8, pp. 3779-3787, Aug. 2013.

[10] R. J. Wai and R. Y. Duan, "High-efficiency bidirectional converter for power sources with great voltage diversity," *IEEE Trans. Power Electron.*, vol. 22, no. 5, pp. 1986-1996, Sep. 2007.

[11] Y.-P. Hsieh, J.-F. Chen, L.-S. Yang, C.-Y. Wu, and W.-S. Liu, "High-conversion-ratio bidirectional DC-DC converter with coupled-inductor," *IEEE Trans. Ind. Electron.*, vol. 61, no. 1, pp. 210-222, Jan. 2014.

[12] H. Li, F. Z. Peng, and J. S. Lawler, "A natural ZVS medium-power bidirectional dc-dc converter with minimum number of devices," *IEEE Trans. Ind. Appl.*, vol. 39, no. 2, pp. 525-535, Mar./Apr. 2003.

[13] F. Z. Peng, H. Li, G. J. Su, and J. S. Lawler, "A new ZVS bidirectional dc-dc converter for fuel cell and battery application," *IEEE Trans. Power Electron.*, vol. 19, no. 1, pp. 54-65, Jan. 2004.

[14] G. Ma, W. Qu, G. Yu, Y. Liu, N. Liang, and W. Li, "A zero-voltage-switching bidirectional dc-dc converter with state analysis and soft-switching-oriented design consideration," *IEEE Trans. Ind. Electron.*, vol. 56, no. 6, pp. 2174-2184, Jun. 2009.

[15] K. Wu, C. W. de Silva, and W. G. Dunford, "Stability analysis of isolated bidirectional dual active full-bridge dc-dc converter with triple phase-shift control," *IEEE Trans. Power Electron.*, vol. 27, no. 4, pp. 2007-2017, Apr. 2012.

[16] S. Inoue and H. Akagi, "A bidirectional dc-dc converter for an energy storage system with galvanic isolation," *IEEE Trans. Power Electron.*, vol. 22, no. 6, pp. 2299-2306, Nov. 2007.

[17] Y. Xie, J. Sun, and J. S. Freudenberg, "Power flow characterization of a bidirectional galvanically isolated high-power dc/dc converter over a wide operating range," IEEE Trans. Power Electron., vol. 25, no. 1, pp. 54-66, Jan. 2010.

[18] H.-J. Choi, W.-B. Lee, and J.-H. Jung, "Practical Design Methodology of Dual Active Bridge Converter as Isolated Bi-directional DC-DC Converter for Solid State Transformer," *The Transactions of the Korean Institute of Power Electronics*, vol. 22, no. 2, pp. 102-108, Apr. 2017.

[19] L. Zhu, "A novel soft-commutating isolated boost full-bridge ZVS-PWM dc-dc converter for bidirectional high power applications," *IEEE Trans. Power Electron.*, vol. 21, no. 2, pp. 422-429, Mar. 2006.

[20] T. F. Wu, Y. C. Chen, J. G. Yang, and C. L. kuo, "Isolated bidirectional full-bridge dc-dc converter with a flyback snubber," *IEEE Trans. Power Electron.*, vol. 25, no. 7, pp. 1915-1922, Jul. 2010.

[21] G. Chen, Y. S. Lee, S. Y. R. Hui, D. Xu, and Y. Wang,

"Actively clamped bidirectional flyback converter," *IEEE Trans. Ind. Electron.*, vol. 47, no. 4, pp. 770-779, Aug. 2000.
[22] F. Zhang and Y. Yan, "Novel forward-flyback hybrid bidirectional dc-dc converter," *IEEE Trans. Ind. Electron.*, vol. 56, no. 5, pp. 1578-1584, May. 2009.
[23] A. S. Samosir and A. H. M. Yatim, "Implementation of dynamic evolution control of bidirectional dc-dc converter for interfacing ultracapacitor energy storage to fuel-cell system," *IEEE Trans. Ind. Electron.*, vol. 57, no. 10, pp. 3468-3473, Oct. 2010.
[24] M. B. Camara, H. Gualous, F. Gustin, A. Berthon, and B. Dakyo, "DC/DC converter design for super-capacitor and battery power management in hybrid vehicle applications — Polynomial control strategy," *IEEE Trans. Ind. Electron.*, vol. 57, no. 2, pp. 587-597, Feb. 2010.
[25] L. R. Chen, N. Y. Chu, C. S. Wang, and R. H. Liang, "Design of a reflex-based bidirectional converter with the energy recovery function," *IEEE Trans. Ind. Electron.*, vol. 55, no. 8, pp. 3022-3029, Aug. 2008.
[26] H.-C. Park and I.-S. Kim, "Bi-directional Buck-Boost Converter Controller Design Method for ESS using Matlab SISO TOOL," *The Transactions of the Korean Institute of Power Electronics*, vol. 21, no. 6, pp. 457-464, Dec. 2016.
[27] K. Jin, M. Yang, X. Ruan, and M. Xu, "Three-level bidirectional converter for fuel-cell/battery hybrid power system," *IEEE Trans. Ind. Electron.*, vol. 57, no. 6, pp. 1976-1986, Jun. 2010.
[28] F. Z. Peng, F. Zhang, and Z. Qian, "A magnetic-less dc-dc converter for dual-voltage automotive systems," *IEEE Trans. Ind. Appl.*, vol. 39, no. 2, pp. 511-518, Mar./Apr. 2003.
[29] I. D. Kim, S. H. Paeng, J. W. Ahn, E. C. Nho, and J. S. Ko, "New bidirectional ZVS PWM sepic/zeta dc-dc converter," in *Proc. IEEE ISIE*, 2007, pp. 555-560.
[30] Y. S. Lee and Y. Y. Chiu, "Zero-current-switching switched-capacitor bidirectional dc-dc converter," *Proc. Inst. Elect. Eng. — Elect. Power Appl.*, vol. 152, no. 6, pp. 1525-1530, Nov. 2005.
[31] R. J. Wai and R. Y. Duan, "High-efficiency bidirectional converter for power sources with great voltage diversity," *IEEE Trans. Power Electron.*, vol. 22, no. 5, pp. 1986-1996, Sep. 2007.
[32] H. Wu, J. Lu, W. Shi, and Y. Xing, "Nonisolated bidirectional dc-dc converters with negative coupled inductor," *IEEE Trans. Power Electron.*, vol. 27, no. 5, pp. 2231-2235, May 2012.

Chang-Soon Lim He received the B.S. degree in electronic engineering from Soongsil University, Seoul, Korea, in 2009, and the M.S. and Ph.D. degrees in electrical engineering from Hanyang University, Seoul, Korea, in 2011 and 2014, respectively. Since 2014, he has been with the Mechatronics R&D Center, Samsung Electronics Company, Ltd., Hwaseong, Korea. His research interests include modeling and control of power converter systems for renewable energies and battery charger.

Kui-Jun Lee He received the B.S. and Ph.D. degrees in electrical engineering from Hanyang University, Seoul, Korea, in 2005 and 2012, respectively. From 2012 to 2014, he was a Post-doctoral Researcher at FREEDM Systems Center, North Carolina State University, Raleigh, NC, USA. From 2014 to 2016, he was a Senior Engineer at Samsung Electronics, Suwon, Korea. Since 2016, he has been with Korea National University of Transportation, where he is currently an Assistant Professor in the Department of Electrical Engineering. His research interests include power converter system for renewable energies and soft-switching techniques.